Journal of Magnetic Resonance 301 (2019) 85–93

Contents lists available at ScienceDirect

Journal of Magnetic Resonance

journal homepage: www.elsevier.com/locate/jmr

Diffusional attenuation during soft pulses: A Zangger-Sterk pure shift iDOSY experiment

Maria Grazia Concilio [a], Peter Kiraly [b], Gareth A. Morris [b,*]

[a] School of Chemistry, University of Southampton, University Road, Southampton SO17 1BJ, UK
[b] School of Chemistry, University of Manchester, Oxford Road, Manchester M13 9PL, UK

ARTICLE INFO

Article history:
Received 25 November 2018
Revised 27 February 2019
Accepted 28 February 2019
Available online 2 March 2019

Keywords:
SPINACH
Spin dynamics simulation
Fokker-Planck formalism
DOSY
Pure shift NMR
Zangger-Sterk iDOSY

ABSTRACT

Diffusion-ordered spectroscopy experiments in which existing delays in a parent pulse sequence are used for diffusion encoding – iDOSY experiments – are potentially attractive because of their simplicity and sensitivity. However the calculation of diffusional attenuation in Zangger-Sterk pure shift iDOSY experiments is a very difficult problem to attack analytically, and is more easily approached numerically. Numerical simulations show that for typical experimental conditions, the dependence of diffusional attenuation on diffusion-encoding gradient amplitude is well represented by a shifted Gaussian function. The shift in gradient can be calculated analytically for the limiting case where the selective pulse is replaced by a hard 180° pulse at its midpoint; numerical simulations show that the effect of using different shapes of selective pulse is to scale down this limiting gradient shift by a constant factor that depends on the pulse shape used. The practical consequence is that under the experimental conditions appropriate for small molecules, the pure shift iDOSY method should allow good diffusion coefficient measurements to be made if appropriate allowance is made for the change in effective diffusion-encoding gradient. Parallel sets of numerical simulations and experiments are presented, and a practical application of a Zangger-Sterk pure shift iDOSY experiment to a simple test mixture is illustrated.

1. Introduction

Diffusion-ordered spectroscopy (DOSY) is widely used for mixture analysis, but the quality of results in the diffusion dimension is critically limited by spectral resolution [1–3]. One of the most powerful ways to improve such resolution is by the use of broadband homonuclear decoupling or "pure shift" methods [4–6]; indeed one of the initial stimuli to the development of such methods was the need for improved spectral resolution in DOSY [7,8]. The majority of current pure shift NMR methods map out the chemical shift evolution using an evolution period which has a hard 180° pulse and an "active spin refocusing" element at its midpoint, the combined effect of which is to refocus the effects of homonuclear couplings [4–6]. The archetypal active spin refocusing element is that of Zangger and Sterk (ZS) [9], which consists of a selective 180° radiofrequency pulse in the presence of a weak constant magnetic field gradient along the *z* axis. The effect of the ZS element is both spatially and spectrally selective, refocusing each signal in a spectrum in a different horizontal slice of the active volume of the sample. If only signals from these slices (the "active" spins) are recorded, the combined effect of the ZS element and the hard 180° pulse is that each chemical shift is measured from a different slice of the sample, with its magnetization appearing to evolve continuously over the evolution period. The hard 180° pulse ensures that all the remaining ("passive") spins are inverted halfway through the evolution period, causing evolution of the active spins under homonuclear scalar couplings to be refocused.

Since the soft pulses used in the ZS element have typical durations of the order of tens of ms, comparable to typical diffusion-encoding delays in DOSY experiments, it is very attractive to convert a pure shift NMR experiment into a DOSY experiment by adding incremented diffusion-encoded gradient field pulses on either side of the ZS element. This is an example of internal ("iDOSY") diffusion encoding, a principle which has been used both in various 3D iDOSY experiments [10–13] and in a pure shift iDOSY experiment [8] using the PSYCHE active spin refocusing element [14–16]. The attraction of the iDOSY approach lies both in its simplicity, and in the sensitivity advantage it enjoys through using a spin echo, which retains all of the initial magnetization, rather than a simulated echo, which sacrifices half. The simple concatenation of a DOSY and pure shift experiment would also lead to greater relaxation losses. Fig. 1a shows a simple prototype pulse sequence for a ZS-iDOSY experiment.

* Corresponding author.
E-mail address: g.a.morris@manchester.ac.uk (G.A. Morris).

https://doi.org/10.1016/j.jmr.2019.02.010
1090-7807/

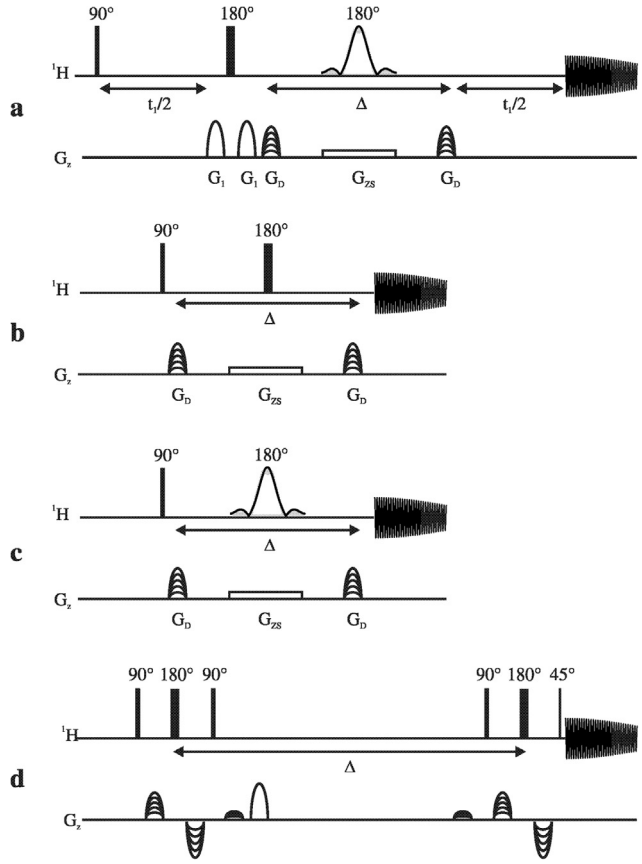

Fig. 1. Pulse sequences. Semi-ellipses represent half-sine shaped gradient pulses; overlaid semi-ellipses indicate incremented diffusion-encoding gradient pulses of amplitude g_D. The diffusion-encoding gradient pulses (g_D) are of duration δ and the Zangger-Sterk gradient pulse (g_{ZS}) and selective 180° pulse are both of duration τ_{ZS}. (a) prototype Zangger-Sterk iDOSY sequence; (b) idealised sequence in which an instantaneous inversion is applied midway through the ZS gradient pulse g_{ZS}; (c) model sequence which omits the evolution period and hard 180° pulse from sequence (a) (the experiments of Fig. 2 used rectangular gradient pulses for consistency with the simulations); and (d) Oneshot-45 sequence [31]. Four different shaped 180° soft pulses (rectangular, Gaussian, RSNOB, REBURP) were used. Sequence (a) uses double EXORCYCLE phase cycling, sequences (b) and (c) normal EXORCYCLE. Pulse sequence code for Bruker spectrometers, with full phase cycling, for sequences (a), (c) and (d) is included in the accompanying Supporting Information.

There is, however, a significant obstacle to the use, or at least the quantitative use, of ZS-iDOSY experiments. This is the difficulty of determining an accurate diffusion coefficient from the signal attenuation measured as a function of diffusion-encoding pulsed field gradient strength. In existing DOSY experiments the form of this attenuation can be found analytically, as first demonstrated by Stejskal and Tanner [17] for the pulsed field gradient spin echo sequence and subsequently extended to a wide variety of other experiments [18]. In such experiments all changes of coherence order can safely be approximated as occurring instantaneously, all the spins observed follow the same coherence transfer pathway as a function of time, and all parts of the sample contribute to the signals observed. However in the case of a ZS-iDOSY experiment none of these is true: the use of a soft pulse means that the process of coherence transfer takes many milliseconds (meaning that diffusion during this process contributes to signal attenuation); spins with different chemical shifts and different spatial positions will have different coherence histories (meaning that the total signal decay observed will have a range of contributions with different functional forms); and the signals observed are confined to those from the thin horizontal slices of sample for which the soft pulse causes refocusing.

Calculation of the diffusional attenuation expected in a ZS-iDOSY experiment is therefore analytically intractable. At first sight, then, it would appear that ZS-iDOSY experiments would at best be limited to use with qualitative interpretation only, dispersing signals according to their relative diffusion coefficients but without the benefit of the absolute diffusion scale available in other DOSY experiments. However, the recent major advances in simulation methods in magnetic resonance, and in particular the implementation of Fokker-Planck methods in the SPINACH platform [19,20], hold out the possibility that numerical modelling might provide sufficient insight into the functional form of the diffusional attenuation in ZS-iDOSY experiments to make it possible to derive diffusion coefficients with sufficient accuracy for practical applications. Here it is demonstrated that this is indeed the case, and that with a minor modification to current data processing methods it is possible to produce iDOSY spectra with accurate diffusion scales. A series of simulations is explored, a simple functional form for the diffusional attenuation is deduced that is applicable over a wide range of experimental parameters, and a practical illustration of the use of ZS-iDOSY to give a very high resolution ^{1}H DOSY spectrum is provided.

1.1. Diffusional attenuation

An obvious starting point for an heuristic analysis of diffusional attenuation in ZS-iDOSY experiments is to calculate the diffusional attenuation $A(g_D)$ as a function of diffusion-encoding gradient pulse amplitude g_D for a limiting case in which the effect of the soft pulse is approximated by an instantaneous 180° rotation at its midpoint. For such a sequence, shown in Fig. 1b, none of the three obstacles to analytical derivation noted above applies, and conventional methods ([17], see Appendix A) yield the diffusional attenuation, Eq. (1):

$$A(g) = \frac{S(g_D)}{S(\Delta g_0)} = e^{-[\gamma\sigma\delta(g_D-\Delta g_0)]^2 D\Delta'} \quad (1)$$

where $S(g_D)$ is the signal measured for a gradient amplitude g_D, γ is the magnetogyric ratio, δ is the duration of the field gradient pulses, σ is a gradient pulse shape factor (which is less than unity for non-rectangular pulses), D is the diffusion coefficient, and Δ' is the diffusion delay corrected for diffusion during the gradient pulses. For rectangular gradient pulses $\sigma = 1$ and $\Delta' = \Delta - \delta/3$, and for half-sine shaped pulses $\sigma = 2/\pi$ and $\Delta' = \Delta - \delta/4$. The difference between Eq. (1) and the normal Stejskal-Tanner equation lies in the gradient shift Δg_0, which is given by Eq. (2):

$$\Delta g_0 = -\frac{g_{ZS}\tau_{ZS}^2}{4\sigma\delta\Delta'} \quad (2)$$

where g_{ZS} is the amplitude of the slice-selection Zangger-Sterk field gradient pulse and τ_{ZS} the duration of the ZS gradient pulse and radiofrequency soft pulse. The diffusional attenuation remains Gaussian in form, but the effect of the Zangger-Sterk gradient is to shift the signal maximum away from $g_D = 0$. This is because the extra field gradient pulse will tend either to enhance the dephasing effect of the diffusion-encoding gradient pulse, or to refocus it, depending on the signs of the two gradient amplitudes.

How closely the diffusional attenuation in a given ZS-iDOSY experiment approaches this ideal limit will depend on the shape of the selective pulse used and on the details of the magnetization trajectory during it. A pulse in which the radiofrequency amplitude is concentrated close to the midpoint (e.g. RSNOB [21]) will be closer to the limit, a pulse in which the radiofrequency amplitude is more evenly distributed (e.g. a rectangular pulse) will be further from it. An optimist might then suggest that the diffusional attenuation to be anticipated for a given selective pulse shape would be

of the same form as Eq. (1), but with a gradient shift Δg_0 which is scaled down by some factor α. As is shown below, such optimism is well-founded.

2. Materials and methods

2.1. Theory

Recent additions to the *Spinach* software package [19,20] have provided the numerical infrastructure for simulating spatiotemporal NMR experiments, including pure shift NMR [4–6], ultrafast NMR [22], slice selection in magnetic resonance imaging (MRI) [23], and Thrippleton-Keeler zero-quantum suppression [24]. The method used is based on the Fokker-Planck equation, Eq. (3):

$$\frac{\partial\rho(x,t)}{\partial t} = -iL(x,t)\rho(x,t) + M(x,t)\rho(x,t) \tag{3}$$

where $\rho(x,t)$ is the average density matrix at every point x in space, $L(x,t) = H(x,t) + iR + iK$ is the Liouvillian responsible for the spin dynamics of a quantum system in which R and K are the relaxation and kinetic operators, and $M(x,t)$ is the spatial dynamics generator that controls diffusion and flow. The Fokker-Planck equation allows simulation of experiments in which spatial dynamics (*i.e.* diffusion and flow) occur simultaneously with quantum mechanical evolution. The advantages of this method are that the diffusion operator is a constant term in the background Hamiltonian, and the radiofrequency fields have time-independent generators. Computations using Eq. (3) make use of the matrix representation of its constituent operators, allowing problems to be easily treated without time-consuming Monte-Carlo sums over stochastic trajectories [25].

In the *Spinach* software, spatial coordinates are discretized on finite grids so that all the differential operators become finite difference matrices. In order to achieve accurate calculation of the evolution caused by pulsed field gradients, the appropriate number of grid points and stencil size have to be determined. Appropriate accuracy (yielding an error in diffusion coefficient below 0.1–0.2%) can be obtained using a 5–7 point stencil size and a spatial grid spacing less than one seventh of the gradient helix pitch. Simulations in this work were therefore performed using a 7-point stencil size and 20,000 grid points; convergence was checked by repeating sample calculations with successively finer digitization.

A series of numerical simulations of diffusional attenuation for a uniform sample of diffusion coefficient 1.80×10^{-9} m^2 s^{-1} in uniform radiofrequency and static magnetic fields was carried out using Spinach version 2.1.4619, for the pulse sequence of Fig. 1b with four different soft pulse shapes (rectangular, Gaussian [26,27], RSNOB [21] and REBURP [28]), three different selective pulse durations τ_{ZS} (30, 45 and 60 ms), and six different Zangger-Sterk gradient amplitudes g_{ZS} (±1%, ±2% and ± 3% of 0.53 T m^{-1}). The diffusion delay Δ was 0.1 s and the diffusion-encoding gradient pulses were of 2 ms duration and rectangular shape, and varied in amplitude from 0.026 to 0.355 T m^{-1} in 16 steps of equal gradient squared. Apparent diffusion coefficients and gradient shifts Δg were extracted from the diffusion decays by least-squares fitting using the Levenberg-Marquardt algorithm implemented in MATLAB (R2017b). Simulations were performed on a MacBook Pro, OS version 10.9.5, 2.9 GHz Intel Core i7, with 8 GB of memory. The set of codes to perform this analysis is included in the accompanying data and software package at DOI: https://doi.org//10.17632/kfc9rgy4cm.1, and will be publicly available in Spinach version 2.3 and later.

2.2. Experimental

A parallel series of experiments was carried out at 25 °C on a 1% w/w solution of H_2O in D_2O doped with $CuSO_4$ to reduce the proton T_1 to 0.2 s at 25 °C and 500 MHz, using a 500 MHz Bruker Neo spectrometer equipped with an RT-DR-BF/1H-5 mm-Z SmartProbe. The pulse sequence of Fig. 1c was used with the same four soft pulse shapes, three selective pulse durations, and six Zangger-Sterk gradient amplitudes g_{ZS} (±1%, ±2% and ±3% of the maximum available gradient). The manufacturer's nominal value for the maximum gradient is 0.535 T m^{-1}, and all nominal experimental gradient strengths are reported with respect to this maximum. The actual signal-weighted root mean square average over the active volume of the sample in the probe used is, as determined below, 0.498 T m^{-1}. The diffusion delay Δ was 0.1 s and the diffusion-encoding gradient pulses were of 2 ms duration and rectangular shape, and varied in amplitude from 0.026 to 0.355 T m^{-1} nominal gradient strength in 16 steps of equal gradient squared. (These gradient values differ slightly from those in the simulations described above; the latter used a nominal diffusion coefficient of 1.8×10^{-9} m^2 s^{-1} rather than the literature value for 1% w/w H_2O in D_2O at the temperature used, 1.906×10^{-9} m^2 s^{-1}, so the experimental gradient amplitudes used were adjusted to give approximately the same pattern of attenuation as the calculations. One data point was omitted from the analysis for each of the experiments using a g_{ZS} of −3% of maximum, to avoid the effects of accidental refocusing of an unwanted coherence transfer pathway at this value of g.

In order to map the spatial variation in the z direction of the field gradient in the probe used, a second series of experiments was performed on the doped water sample, using the pulse sequence of Fig. 1c with a 37 ms RSNOB radiofrequency pulse applied under a field gradient of 1.2% of the maximum available. The transmitter offset was varied from −3050 to +3150 Hz in 125 steps of 50 Hz, to span the full height of the active volume of the sample, and two different values of nominal diffusion-encoding field gradient, 16 and 60% of the maximum available, were used. The diffusion-encoding gradient pulses were of half-sine shape and 1 ms duration, and the diffusion-encoding delay Δ was of 0.1584 s duration. The diffusional attenuation as a function of offset was used to calculate the relative gradient strength as a function of offset, and thence using the known diffusion coefficient of 1.906×10^{-9} m^2 s^{-1} to calculate both the absolute gradient strength, and the relative signal amplitude, as a function of position.

As an illustration of the use of ZS-iDOSY, experiments were carried out on a sample containing 100 mM each of quinine, geraniol and camphene and 5 mM tetramethylsilane in dimethylsulfoxide d_6, using the iDOSY pulse sequence of Fig. 1a and the Oneshot-45 sequence of Fig. 1d. In both cases half-sine shaped diffusion-encoding gradient pulses were used, of 1.4 ms duration for Oneshot-45 and 2.4 ms for iDOSY; the latter used a diffusion delay Δ of 147.1 ms, while Oneshot-45 used 75 ms. For the ZS-iDOSY experiment 32 transients of 0.328 s acquisition time and 10 kHz spectral width were acquired for each of 16 increments in t_1 and 16 increments in diffusion-encoding gradient strength, with nominal amplitudes from 0.068 to 0.273 T m^{-1} in equal steps of gradient squared, in a total time of 7.5 h. (This was rather longer than necessary; an infelicity in the Bruker TopSpin software used (version 4.0.5) requires that the same number of increments be used in both the pure shift and diffusion dimensions of an interferogram-based pure shift DOSY experiment). For the Oneshot-45 experiment 32 transients of 1.638 s acquisition time and 10 kHz spectral width were acquired for each of 8 diffusion-encoding gradient amplitudes, with nominal amplitudes from 0.034 to 0.273 T m^{-1} in equal steps of gradient squared, in a total

time of 0.5 h. The Oneshot-45 data were processed using the VnmrJ 2.2C software package, with correction for the effects of gradient non-uniformity [29,30]. The Zangger-Sterk iDOSY data were processed in the same package, with correction for diffusion during the ZS sequence element using Eqs. (1) and (2) above, followed by correction for the spatial non-uniformity of the *z* gradient using the gradient calibration as a function of position determined as described in the preceding paragraph. All experimental data, pulse sequence code, VnmrJ macros and the Mathematica notebook used are freely available for download from DOI: https://doi.org//10.17632/kfc9rgy4cm.1.

3. Results and discussion

Fig. 2 compares representative examples of the results of simulations and experimental measurements of diffusional attenuation, carried out with the pulse sequence of Fig. 1c for the case of a Gaussian soft pulse shape with different experimental parameters. Normalized diffusional attenuations are marked with black symbols, and fits to a Gaussian with solid and dashed lines, for measurements with Zangger-Sterk gradient strengths of ±1% and ±3% of maximum (0.535 T m^{-1}) respectively. Corresponding plots are given for the complete set of simulation and experiment results in the accompanying Supporting Information (SI). The experimental and simulated data show that the diffusional attenuation is indeed well represented by a Gaussian over the range of experimental parameters explored, which is typical of the conditions likely to be used in practice for ^{1}H ZS-iDOSY experiments. The graphs show the diffusion-encoding gradient increasing from left to right on the right hand half of each subplot, where the ZS gradient is positive, and from right to left on the left hand half, where the ZS gradient is negative. (In the absence of any instrumental imperfection, the same form of plot would be obtained for the complementary case where the ZS gradient is kept positive but the diffusion-encoding gradient varies over the full range from negative to positive). The experimental data show slightly different gradient shifts Δg_0 from the simulations; these are to be expected because of the *ca.* 5% difference between the diffusion coefficient assumed in the simulations and that of the experimental sample used, but will also reflect the fact that the experimental maximum field gradient varies between 0.480 and 0.509 T m^{-1} over the active volume of the sample (see below).

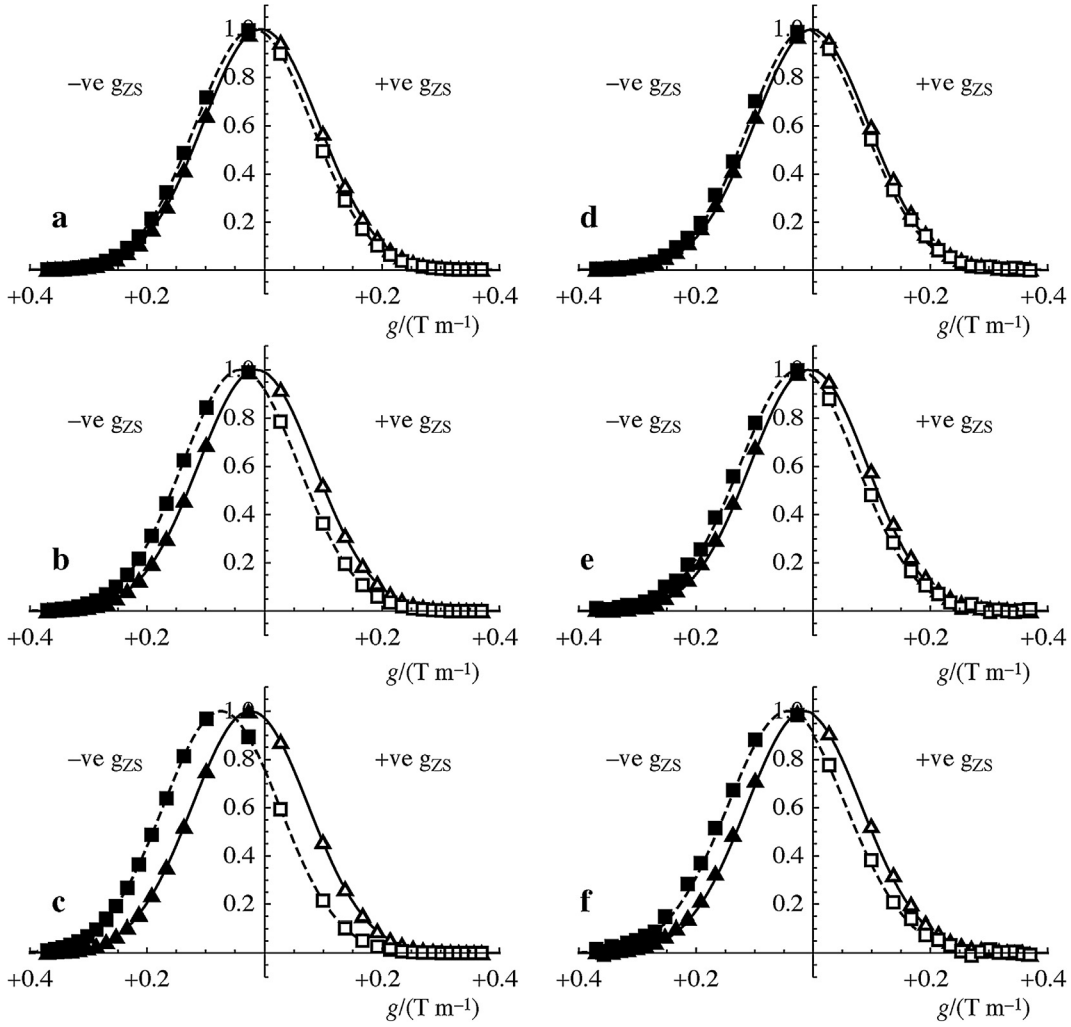

Fig. 2. Normalized diffusional attenuation curves observed in simulations (left column, a–c) and experiments (right column, d–f) with the pulse sequence of Fig. 1c, using Gaussian soft pulses of duration 30 ms (a and d), 45 ms (b and e) and 60 ms (c and f). Calculated and experimental points are shown as squares for a g_{ZS} of ±3% of maximum and triangles for ±1%, with the symbols open for positive g_{ZS} and filled for negative. Gaussian fits are shown as solid lines for ±3% g_{ZS} and dashed lines for ±1%. The maximum gradient amplitude was 0.53 T m^{-1} for simulations, and between 0.515 and 0.534 T m^{-1} depending on position within the active volume of the sample for experiments. Simulations used a diffusion coefficient of 1.8×10^{-9} m^2 s^{-1}, while the experimental sample had a literature diffusion coefficient of 1.906×10^{-9} m^2 s^{-1}. Details of the fits are given in the text.

The diffusional attenuation data for positive and negative ZS gradients were fitted independently, but in the great majority of cases the fits for positive and negative ZS gradient show excellent consistency. The one exception is for experimental measurements with a ZS gradient of +3% (several times that normally used for ^{1}H NMR experiments at 500 MHz). There is a very small discrepancy, barely visible in Fig. 2f, between the amplitudes of the fitted positive and negative half-Gaussians; the corresponding discontinuity is greater for the other three shapes of soft pulse (see the corresponding figures in the SI). This inconsistency between fits for the positive and negative ZS gradient data arises because the gradient shift Δg_0 for positive ZS gradient is so large that these experimental data show only the tail of the Gaussian shape, and hence do not allow reliable fitting at the signal-to-noise ratio available.

The simulated and experimental data also confirm that different soft pulse shapes give rise to different correction factors α in Eq. (2). Fig. 3 shows a plot of the magnitudes of the gradient shifts Δg found by Gaussian fitting of the simulated data against those of the shifts Δg_0 given by Eq. (2) with $\alpha = 1$ for the ideal case of an instantaneous inversion at the midpoint of the ZS gradient pulse. Excellent agreement is seen with Eq. (2), the values of α for the Gaussian, rectangular, RSNOB and REBURP soft pulse shapes being 0.98, 1.46, 1.02 and 1.04 respectively. As expected, the values for Gaussian, RSNOB and REBURP pulse shapes, where the radiofrequency power is concentrated close to the midpoint of the selective pulse, are close to unity, while a much larger value is obtained for rectangular pulses, where the spin trajectories are perturbed throughout the pulse duration.

Although, as seen above and in the SI, the form of the diffusional attenuation seen in the simulations remains close to Gaussian, the width of the Gaussian differs slightly from that in the corresponding Stejskal-Tanner expression, and hence the fitted apparent diffusion coefficients obtained for the simulated data differ slightly from that used as input to the simulation. For small gradient shifts (*i.e.* short soft pulses, weak ZS gradient g_{ZS}) the error in diffusion coefficient is small; with larger Δg the error increases roughly quadratically, with a magnitude that depends on the pulse shape used. Again, the deviation from the predicted result follows different trends for the different soft pulses investigated. Interestingly, the sign of the (small) error for Gaussian pulses is opposite to that for the other three pulse shapes. The magnitude of the deviation in D depends on the ratio of the gradient shift Δg to the change in gradient amplitude needed to effect a given change in diffusional attenuation. As Fig. 4 shows, for small Δg the width of the Gaussian is very close to that for the normal Stejskal-Tanner equation with $\Delta g_0 = 0$, allowing diffusion coefficients to be deduced directly from fits. For large Δg the value of D obtained by fitting needs to be divided by a scaling factor β that depends on the soft pulse shape. β is well-represented by a quartic function of Δg; a the full list of parameters obtained from the quartic fit for each soft pulse shape is reported in the SI.

If the diffusion-encoding gradient amplitude g at which signal attenuation reaches 50% is $g_{1/2}$, then for $\Delta g \leq 0.6\, g_{1/2}$ the difference between the diffusion coefficient obtained by Gaussian fitting of the diffusional attenuation and the true value is of the order of 1% or less for Gaussian, RSNOB and REBURP pulses, but *ca.* 16% for rectangular. For practical experiments, therefore, which use pulses shaped to give largely positive excitation spectra, the correction factor β is only needed for cases where $\Delta g > 0.6\, g_{1/2}$.

In summary, experimental conditions should normally be chosen to use shaped pulses such as Gaussian, RSNOB or REBURP, and values of δ, Δ and g_{ZS} for which $\Delta g < 0.6\, g_{1/2}$. The latter condition ensures that the diffusional attenuation is dominated by the diffusion-encoding gradient pulses, so that the only change to normal practice needed is to calculate Δg from the experimental parameters and the known scaling factor for the pulse shape, and use normal two-parameter fitting but with gradient amplitude values shifted by an amount $\Delta g_0/\alpha$. In principle it would alternatively be possible to move from two- to three-parameter fitting, treating Δg as a variable parameter, but this would involve a significant sacrifice in the accuracy of fitting for D.

There is however a practical complication if accurate results are to be obtained using iDOSY experiments. As noted earlier, the pulsed field gradients produced by commercial NMR equipment are not completely homogeneous: the magnitude of the gradient varies with position within the active volume of the sample.

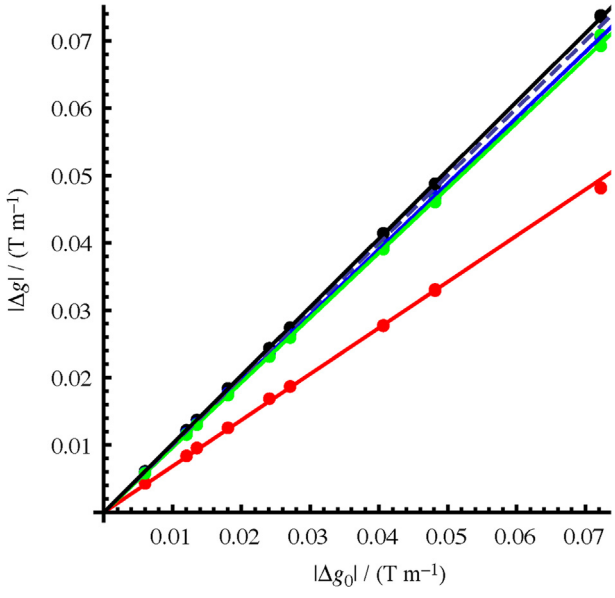

Fig. 3. Gradient shift magnitudes $|\Delta g|$ (filled circles) determined by fitting of the results of the simulations of diffusional attenuation, plotted against the corresponding gradient shift magnitudes $|\Delta g_0|$ calculated from Eq. (2) with $\sigma = 1$, the ideal limit of instantaneous 180° rotation at the midpoint of the radiofrequency selective pulse. The dotted line shows the 45° slope $|\Delta g| = |\Delta g_0|$, and solid lines show lines of best fit $|\Delta g| = |\Delta g_0|/\alpha$ passing through the origin, for (in order of increasing slope) rectangular (red), REBURP (green), RSNOB (blue) and Gaussian (black) radiofrequency soft pulses. (For interpretation of the references to color in this figure legend, the reader is referred to the web version of this article.)

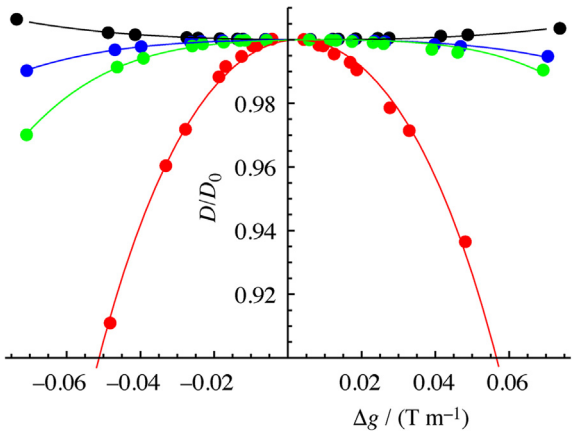

Fig. 4. Ratio D/D_0 of fitted to input diffusion coefficient as a function of the fitted gradient shift Δg for the four types of soft radiofrequency pulse used. Filled circles show calculated data points, solid lines polynomial fits (using quadratic and quartic terms) for, in order of increasingly negative deviation, Gaussian (black), RSNOB (blue), REBURP (green) and rectangular (red) soft pulses. (For interpretation of the references to color in this figure legend, the reader is referred to the web version of this article.)

Different manufacturers have historically chosen different compromises between the uniformity of the field gradient and the speed with which it can be changed. Thus Varian/Agilent room temperature probes typically show a gradient variation of as much as 20% across the sample volume, but have sufficiently short rise and fall times that rectangular gradient pulse shapes can be used, while Bruker room temperature probes typically show only 4–5% variation in g but normally have to use half-sine shaped gradient pulses.

In conventional DOSY experiments the only effect of spatial non-uniformity of the field gradient is to cause the form of the diffusional attenuation as a function of gradient strength to differ slightly from that of the Stejskal-Tanner equation (Eq. (1) with $\Delta g_0 = 0$). With Bruker probes this effect can normally be neglected, but with Varian probes non-uniform gradient correction is helpful where accurate diffusion coefficients, and the best resolution in the diffusion domain of a DOSY spectrum, are required [29,30]. In the case of spatially-resolved DOSY experiments such as ZS-iDOSY, however, even relatively small spatial variations in g will have a substantial impact on the quality of DOSY spectra, because the spatial variation translates into a variation of apparent diffusion coefficient with offset from resonance. Fortunately it is relatively easy to map, and correct for, gradient non-uniformity. One way to map gradients is to apply a weak read gradient during the acquisition of DOSY data, so that different positions in the sample correspond to different positions within the signal profile as a function of frequency [29,30]. A simple, but slightly slower, alternative that is less demanding of the speed of gradient switching is to perform an iDOSY experiment such as that of Fig. 1c on a sample, such as dilute HDO in D_2O, which has an accurately known diffusion coefficient and a strong signal. Varying the offset from resonance then varies the position of the active slice of spins within the active volume, again mapping the variation of apparent diffusion coefficient with position, but point by point rather than in a single experiment. Given the known timing of the experiment, the appropriate Stejskal-Tanner equation, and the diffusion coefficient of the sample, it is straightforward to calculate the absolute gradient strength as a function of offset from resonance. Since the slice-selection gradient strength g_{ZS} is also known, numerical integration can then be used to derive the gradient (and signal) strength as a function of position (the distance scale being determined by the diffusion coefficient) [30].

Fig. 5 shows the spatial variation of the measured 100% gradient strength as a proportion of the nominal value of 0.535 T m^{-1} specified by the manufacturer, and the relative signal intensity, obtained for the probe used. The signal-weighted root mean square average 100% gradient strength (the value that would give the correct diffusion coefficient for measurements of the whole sample in the limit of an experiment with weak diffusional attenuation) is 0.498 T m^{-1}, very slightly less than the nominal value. A simple polynomial fit (8th order suffices in both cases) of the variation in relative gradient strength and relative signal amplitude as a function of offset from resonance $\Delta\nu$, yielding the functions $R_g(\Delta\nu)$ and $R_A(\Delta\nu)$, allows their respective variations to be corrected for in the construction of a DOSY spectrum. The calibration is probe-specific, but can be used to correct data acquired with different values of g_{ZS} by appropriate scaling in the frequency dimension.

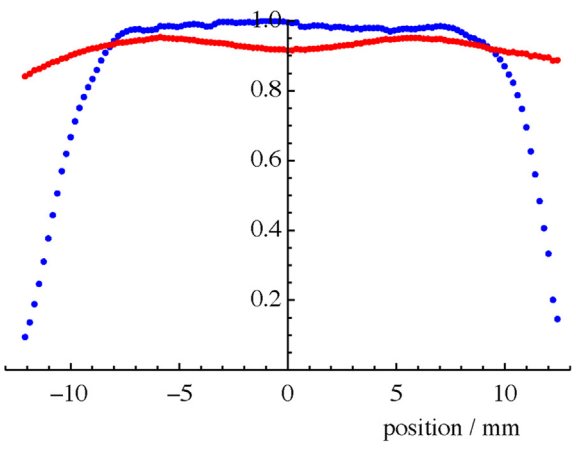

Fig. 5. Relative signal amplitude (upper trace, blue points), and 100% gradient amplitude (lower trace, red points) as a fraction of the nominal value of 0.535 T m^{-1}, as a function of displacement from the field gradient centre in the active volume of the probe coil. (For interpretation of the references to color in this figure legend, the reader is referred to the web version of this article.)

Finally, Fig. 6 compares a conventional DOSY spectrum obtained with the Oneshot-45 pulse sequence [31] of a test sample containing quinine, geraniol, camphene and TMS in dimethylsulfoxide d_6 with a pure shift ZS-iDOSY spectrum obtained using the sequence of Fig. 1a. The former 2D spectrum was obtained by standard methods [1–3], fitting the experimentally measured diffusional attenuation for each peak i to the appropriate form of the Stejskal-Tanner equation, to yield an amplitude A_i, a diffusion coefficient D_i, and the estimated uncertainty in diffusion coefficient σ_{Di}, and then using the table of fitted parameters to construct the DOSY spectrum. The ZS-iDOSY spectrum was obtained in the same way but (a) using the modified Stejskal-Tanner equation Eq. (1) with a gradient shift calculated form Eq. (2) with $\alpha = 1.02$, to reflect the RSNOB pulse used, and (b) with the apparent diffusion coefficient D, uncertainty σ_D in D, and signal amplitude A as a function of offset from resonance corrected using the two polynomials $R_g(\Delta\nu_I)$ and $R_A(\Delta\nu_I)$, obtained as described above. The amplitudes A_i were not corrected for the difference between $S(0)$ and $S(\Delta g_0)$, which is negligible under these conditions, and no correction β was required. The corrected parameters A_i^c, D_i^c and σ_{Di}^c for peak i are

$$A_i^c = A_i R_g(\Delta\nu_I)/R_A(\Delta\nu_I) \tag{4}$$

$$D_i^c = D_i/R_g(\Delta\nu_I)^2 \tag{5}$$

$$\sigma_{Di}^c = \sigma_{Di}/R_g(\Delta\nu_I)^2 \tag{6}$$

In the conventional Oneshot-45 DOSY spectrum of Fig. 6a, overlap between the proton multiplets of the different species is widespread in the region between 5.5 and 1 ppm, with the result that many peaks appear in the DOSY spectrum at apparent diffusion coefficients intermediate between those of the different species involved. This makes the spectrum difficult to interpret, prevents the extraction of clean subspectra for the individual components, and can lead to the unwary user inferring the presence of more species than is the case. In contrast, the ZS-iDOSY spectrum of Fig. 6b shows essentially no signal overlap, with very good consistency in diffusion coefficient between the signals of a given species, and it would be straightforward to extract clean pure shift spectra of quinine, camphene and geraniol by projection of the appropriate regions of the diffusion dimension onto the chemical shift axis. The greater impact of transverse relaxation on the ZS-iDOSY experiment leads to the loss of a number of exchanging signals, including the broad water resonance at 3.4 ppm, in Fig. 6b, contributing further to the simplification of the DOSY spectrum. Intriguingly, the widths of the individual peaks in the diffusion dimension are significantly smaller in Fig. 6b than in Fig. 6a, indicating that the precision of the diffusion coefficients values obtained is significantly greater for the ZS-iDOSY experiment than for Oneshot-45. A similar improvement was reported previously in the case of the PSYCHE-iDOSY experiment [8].

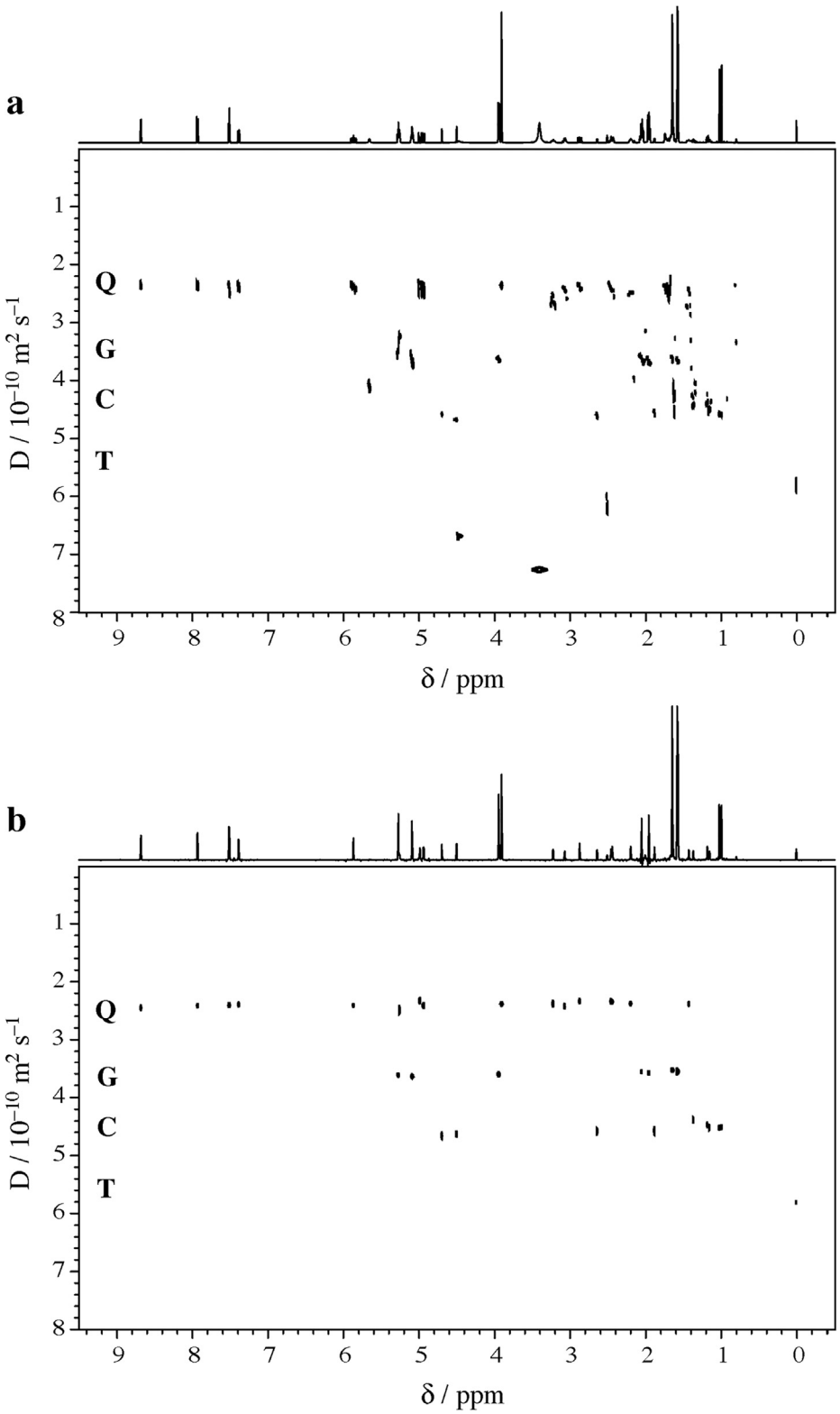

Fig. 6. Oneshot-45 (a) and Zangger-Sterk iDOSY (b) spectra of a 100 mM solution of quinine (Q), geraniol (G) and camphene (C) in dimethylsulfoxide d_6 with 5 mM tetramethylsilane (T) reference.

4. Conclusions

The signal attenuation caused by diffusion in a weak field gradient during a long shaped radiofrequency pulse is not amenable to analytical calculation, but with recent advances in numerical simulation methods it is possible to perform accurate calculations with relatively modest resources. Systematic investigation of the form of signal attenuation in experiments that combine such

spatially- and frequency-selective pulses with strong diffusion-encoding gradient pulses, for example to perform diffusion-ordered spectroscopy experiments with internal diffusion encoding, shows that the diffusional signal attenuation is well represented by a shifted Gaussian function. (A similar form of approximate Stejskal-Tanner equation is used in the PSYCHE-iDOSY pure shift DOSY experiment [5]). The gradient shift here is that calculable analytically for the limiting case of a hard 180° pulse at the midpoint of the applied gradient pulse, scaled down by a factor that depends on the shape of soft pulse used and is close to unity for the shapes most commonly used. If the contribution of the weak gradient is small compared to that of the strong diffusion-encoding gradient pulses, the width of the Gaussian attenuation function remains very close to that seen in the absence of the weak gradient. If this condition is not met, a radiofrequency pulse shape dependent correction for the effect of the weak gradient can be applied.

Practical implementation of experiments using spatially- and frequency-selective pulses in DOSY (Zangger-Sterk-iDOSY experiments) requires that the spatial variation of the applied magnetic field gradient be characterised and corrected for. The gradient can be mapped either by existing methods, or by measuring the diffusional attenuation of a reference material in a ZS-iDOSY experiment as a function of offset from resonance. While the need to apply corrections both for the shifted diffusional attenuation function and for the spatial variation of gradient may at first sight seem onerous, in practice only a single calibration experiment is required, and it is straightforward to make the corrections needed transparent to the end user.

Acknowledgements

The authors gratefully acknowledge Prof Ilya Kuprov, Dr Jean-Nicolas Dumez, Dr Mohammadali Foroozandeh and Dr Mathias Nilsson for many helpful discussions, and Dr Aaron Hernandez-Cid and Mr Guilherme Dal Poggetto for assistance with preliminary experimental work. This work was supported by the Agence Nationale de la Recherche and the EPSRC (grant number EP/N033949).

Appendix A

For a pulse sequence consisting of N intervals of durations t_i during which the field gradient amplitude is g_i and the coherence order p_i, the net gradient encoding and the diffusional attenuation caused will be respectively the sum and the product of terms for the individual intervals [17]. For the i'th interval, the gradient encoding will be

$$q_i = \int_0^{t_i} p_i g_i(t) dt \tag{A1}$$

and the diffusional attenuation contribution

$$a_i = \exp\left[-\gamma^2 D \int_0^{t_i} \left\{ q_{i-1} + p_i \int_0^{t_i} g_i(t')dt' \right\}^2 dt\right] \tag{A2}$$

where $q_0 = 0$.

The pulse sequence of Fig. 1b consists of 6 intervals: a diffusion-encoding gradient pulse of duration δ and amplitude g_D, a delay with no gradient, a delay $\tau_{ZS}/2$ with a gradient g_{ZS}, and then the same three intervals but in reverse order. The coherence order p changes from +1 to −1 at the midpoint, between the two intervals $\tau_{ZS}/2$. For rectangular diffusion-encoding gradient pulses, the calculation of the net gradient area and the diffusional attenuation for this sequence is summarised in Table A1.

The total diffusional attenuation for pulse sequence 1b with rectangular gradient pulses is thus

$$A = S/S_0 = \exp[-\gamma^2 D\{g_{ZS}^2\tau_{ZS}^3 + 6g_D g_{ZS}\tau_{ZS}^2\delta + 4g_D^2\delta^2(3\Delta - \delta)\}/12] \tag{A3}$$

where S_0 is the signal observed when g_D and g_{ZS} are both zero and S when they are nonzero. The exponent of Eq. (A3) can be rearranged ("completing the square") into the form

$$A = S/S_0 = \exp[-\gamma^2\delta^2\Delta' D\{(g_D - \Delta g_0)^2 + \Delta g_0^2(4\Delta' - 3\tau_{ZS})/(3\tau_{ZS})\}] \tag{A4}$$

where

$$\Delta g_0 = -g_{ZS}\tau_{ZS}^2/(4\Delta'\delta) \tag{A5}$$

and

$$\Delta' = \Delta - \delta/3 \tag{A6}$$

giving

$$A = S/S_0 = \exp[-\gamma^2\delta^2\Delta' D\{(g_D - \Delta g_0)^2 + \Delta g_0^2(4\Delta' - 3\tau_{ZS})/(3\tau_{ZS})\}] \tag{A7}$$

Eqs. (A7) and (A5) reduce to Eqs. (1) and (2) respectively in the main text for the rectangular pulse case $\sigma = 1$.

For half-sine shaped diffusion-encoding gradient pulses the corresponding calculation is summarised in Table A2.
This gives

$$\Delta g_0 = -g_{ZS}\pi\tau_{ZS}^2/(8\Delta'\delta) \tag{A8}$$

and

$$\Delta' = \Delta - \delta/4 \tag{A9}$$

and a final attenuation

$$A = S/S_0 = \exp[-\gamma^2\delta^2\Delta' D(4/\pi^2)\{(g_D - \Delta g_0)^2 + \Delta g_0^2(4\Delta' - 3\tau_{ZS})/(3\tau_{ZS})\}] \tag{A10}$$

corresponding again to Eqs. (1) and (2) of the main text but this time with $\sigma = 2/\pi$.

Table A1
Interval numbers, durations, gradient amplitudes, coherence orders, and gradient encoding and diffusional attenuation contributions for the six intervals of the pulse sequence of Fig. 1b with rectangular diffusion-encoding gradient pulses.

i	t_i	g_i	p_i	q_i	$-\ln(a_i)/\gamma^2 D$
1	δ	g_D	1	$g_D\delta$	$g_D^2\delta^3/3$
2	$(\Delta - \delta - \tau_{ZS})/2$	0	1	0	$g_D^2\delta^2(\Delta - \delta - \tau_{ZS})/2$
3	$\tau_{ZS}/2$	g_{ZS}	1	$g_{ZS}\tau_{ZS}/2$	$g_D^2\delta^2\ \tau_{ZS}/2 + g_{ZS}^2\ \tau_{ZS}^3/24 + g_D g_{ZS}\ \tau_{ZS}^2\delta/4$
4	$\tau_{ZS}/2$	g_{ZS}	−1	$-g_{ZS}\tau_{ZS}/2$	$g_D^2\delta^2\ \tau_{ZS}/2 + g_{ZS}^2\ \tau_{ZS}^3/24 + g_D g_{ZS}\ \tau_{ZS}^2\delta/4$
5	$(\Delta - \delta - \tau_{ZS})/2$	0	−1	0	$g_D^2\delta^2(\Delta - \delta - \tau_{ZS})/2$
6	δ	g_D	−1	$-g_D\delta$	$g_D^2\delta^3/3$
Sum				0	$[g_{ZS}^2\ \tau_{ZS}^3 + 6\ g_D g_{ZS}\ \tau_{ZS}^2\delta + 4g_D^2\delta^2(3\Delta - \delta)]/12$

Table A2
Interval numbers, durations, gradient amplitudes, coherence orders, and gradient encoding and diffusional attenuation contributions for the six intervals of the pulse sequence of Fig. 1b with half-sine shaped diffusion-encoding gradient pulses.

i	t_i	g_i	p_i	q_i	$-\ln(a_i)/\gamma^2 D$
1	δ	$g_D \sin(\pi t/\delta)$	1	$2g_D\delta/\pi$	$3g_D^2\delta^3/(2\pi^2)$
2	$(\Delta-\delta-\tau_{ZS})/2$	0	1	0	$2g_D^2\delta^2(\Delta-\delta-\tau_{ZS})/\pi^2$
3	$\tau_{ZS}/2$	g_{ZS}	1	$g_{ZS}\tau_{ZS}/2$	$2\ g_D^2\delta^2\ \tau_{ZS}/\pi^2 + g_{ZS}^2\ \tau_{ZS}^3/24 + g_D g_{ZS}\ \tau_{ZS}^2\delta/(2\pi)$
4	$\tau_{ZS}/2$	g_{ZS}	−1	$-g_{ZS}\tau_{ZS}/2$	$2\ g_D^2\delta^2\ \tau_{ZS}/\pi^2 + g_{ZS}^2\ \tau_{ZS}^3/24 + g_D g_{ZS}\ \tau_{ZS}^2\delta/(2\pi)$
5	$(\Delta-\delta-\tau_{ZS})/2$	0	−1	0	$2g_D^2\delta^2(\Delta-\delta-\tau_{ZS})/\pi^2$
6	δ	$g_D \sin(\pi t/\delta)$	−1	$-2g_D\delta/\pi$	$3g_D^2\delta^3/(2\pi^2)$
Sum				0	$[g_{ZS}^2\ \tau_{ZS}^3\pi^2 + 12\pi\ g_D g_{ZS}\ \tau_{ZS}^2\delta + 12g_D^2\delta^2(4\Delta-\delta)]/(12\pi^2)$

Appendix B. Supplementary material

Supplementary data to this article can be found online at https://doi.org/10.1016/j.jmr.2019.02.010.

References

[1] K.F. Morris, C.S. Johnson, Mobility-ordered 2-dimensional nuclear magnetic resonance spectroscopy, J. Am. Chem. Soc. 114 (1992) 776–777.
[2] C.S. Johnson, Diffusion ordered nuclear magnetic resonance spectroscopy: principles and applications, Prog. Nucl. Mag. Res. Sp. 34 (1999) 203–256.
[3] G.A. Morris, eMagRes, Wiley, Hoboken, 2009, Doi: 10.1002/9780470034590.emrstm0119.pub2.
[4] R.W. Adams, eMagRes, Wiley, Hoboken, 2014, DOI: 10.1002/9780470034590.emrstm1362.
[5] L. Castañar, T. Parella, Broadband H-1 homodecoupled NMR experiments: recent developments, methods and applications, Magn. Reson. Chem. 53 (2015) 399–426.
[6] K. Zangger, Pure shift NMR, Prog. Nucl. Mag. Res. Sp. 86–87 (2015) 1–20.
[7] M. Nilsson, G.A. Morris, Pure shift proton DOSY: diffusion-ordered H-1 spectra without multiplet structure, Chem. Commun. (2007) 933–935.
[8] M. Foroozandeh, L. Castañar, L.G. Martins, D. Sinnaeve, G. Dal Poggetto, C.F. Tormena, R.W. Adams, G.A. Morris, M. Nilsson, Ultrahigh-resolution diffusion-ordered spectroscopy, Angew. Chem. Int. Ed. 55 (2016) 15579–15582.
[9] K. Zangger, H. Sterk, Homonuclear broadband-decoupled NMR spectra, J. Magn. Reson. 124 (1997) 486–489.
[10] B. Vitorge, D. Jeannerat, NMR diffusion measurements in complex mixtures using constant-time-HSQC-IDOSY and computer-optimized spectral aliasing for high resolution in the carbon dimension, Anal. Chem. 78 (2006) 5601–5606.
[11] A.S. McLachlan, J.J. Richards, A.R. Bilia, G.A. Morris, Constant time gradient HSQC-iDOSY: practical aspects, Magn. Reson. Chem. 47 (2009) 1081–1085.
[12] M. Nilsson, A.M. Gil, I. Delgadillo, G.A. Morris, Improving pulse sequences for 3D diffusion-ordered NMR spectroscopy: 2DJ-IDOSY, Anal. Chem. 76 (2004) 5418–5422.
[13] N. Birlirakis, E. Guittet, A new approach in the use of gradients for size-resolved 2D-NMR experiments, J. Am. Chem. Soc. 118 (1996) 13083–13084.
[14] M. Foroozandeh, R.W. Adams, N.J. Meharry, D. Jeannerat, M. Nilsson, G.A. Morris, Ultrahigh-resolution NMR spectroscopy, Angew. Chem. Int. Ed. 53 (2014) 6990–6992.
[15] M. Foroozandeh, R.W. Adams, M. Nilsson, G.A. Morris, Ultrahigh-resolution total correlation NMR spectroscopy, J. Am. Chem. Soc. 136 (2014) 11867–11869.
[16] M. Foroozandeh, G.A. Morris, M. Nilsson, PSYCHE pure shift NMR spectroscopy, Chem-Eur J 24 (2018) 13988–14000.
[17] E.O. Stejskal, J.E. Tanner, J. Chem. Phys. 42 (1965) 288.
[18] D. Sinnaeve, The Stejskal-Tanner equation generalized for any gradient shape-an overview of most pulse sequences measuring free diffusion, Concept Magn. Reson. A 40a (2012) 39–65.
[19] H.J. Hogben, P.J. Hore, I. Kuprov, Multiple decoherence-free states in multi-spin systems, J. Magn. Reson. 211 (2011) 217–220.
[20] I. Kuprov, Fokker-Planck formalism in magnetic resonance simulations, J. Magn. Reson. 270 (2016) 124–135.
[21] Ē. Kupče, J. Boyd, I.D. Campbell, Short selective pulses for biochemical applications, J. Magn. Reson., Ser B 106 (1995) 300–303.
[22] Y. Shrot, B. Shapira, L. Frydman, Ultrafast 2D NMR spectroscopy using a continuous spatial encoding of the spin interactions, J. Magn. Reson. 171 (2004) 163–170.
[23] R.W. Brown, Y.-C.N. Cheng, E.M. Haacke, M.R. Thompson, R. Venkatesan, Magnetic Resonance imaging Physical Principles and Sequence Design, second ed., John Wiley & Sons Inc., Hoboken, 2014.
[24] M.J. Thrippleton, J. Keeler, Elimination of zero-quantum interference in two-dimensional NMR spectra, Angew. Chem. Int. Ed. 42 (2003) 3938–3941.
[25] G. Pileio, J.N. Dumez, I.A. Pop, J.T. Hill-Cousins, R.C.D. Brown, Real-space imaging of macroscopic diffusion and slow flow by singlet tagging MRI, J. Magn. Reson. 252 (2015) 130–134.
[26] R.J. Sutherland, J.M.S. Hutchison, Three-dimensional NMR imaging using selective excitation, J. Phys. E: Sci. Instrum. 11 (1978) 79–83.
[27] C. Bauer, R. Freeman, T. Frenkiel, J. Keeler, A.J. Shaka, Gaussian pulses, J. Magn. Reson. 58 (1984) 442–457.
[28] H. Geen, R. Freeman, Band-selective radiofrequency pulses, J. Magn. Reson. 93 (1991) 93–141.
[29] P. Damberg, J. Jarvet, A. Gräslund, Accurate measurement of translational diffusion coefficients: a practical method to account for nonlinear gradients, J. Magn. Reson. 148 (2001) 343–348.
[30] M.A. Connell, P.J. Bowyer, P.A. Bone, A.L. Davis, A.G. Swanson, M. Nilsson, G.A. Morris, Improving the accuracy of pulsed field gradient NMR diffusion experiments: correction for gradient non-uniformity, J. Magn. Reson. 198 (2009) 121–131.
[31] A. Botana, J.A. Aguilar, M. Nilsson, G.A. Morris, J-modulation effects in DOSY experiments and their suppression: the Oneshot45 experiment, J. Magn. Reson. 208 (2011) 270–278.